

# Long-Term Stability, Biocompatibility, and Magnetization of Suspensions of Isolated Bacterial Magnetosomes

Frank Mickoleit, Cornelia Jörke, Reinhard Richter, Sabine Rosenfeldt, Simon Markert, Ingo Rehberg, Anna S. Schenk, Oliver Bäumchen, Dirk Schüler,\* and Joachim H. Clement\*

Magnetosomes are magnetic nanoparticles biosynthesized by magnetotactic bacteria. Due to a genetically strictly controlled biomineralization process, the ensuing magnetosomes have been envisioned as agents for biomedical and clinical applications. In the present work, different stability parameters of magnetosomes isolated from *Magnetospirillum gryphiswaldense* upon storage in suspension (HEPES buffer, 4 °C, nitrogen atmosphere) for one year in the absence of antibiotics are examined. The magnetic potency, measured by the saturation magnetization of the particle suspension, drops to one-third of its starting value within this year—about ten times slower than at ambient air and room temperature. The particle size distribution, the integrity of the surrounding magnetosome membrane, the colloidal stability, and the biocompatibility turn out to be not severely affected by long-term storage.

## 1. Introduction

Magnetic nanoparticles are of increasing interest for many biomedical and future clinical applications. Examples include their usage as drug carriers, or as agents for magnetic imaging techniques or magnetic hyperthermia.<sup>[1–4]</sup> However, the synthesis of biocompatible nanoparticles with stable magnetic moments and uniform size and shape is still challenging and often requires harsh reaction conditions.<sup>[5,6]</sup> A promising alternative might be provided by magnetosomes, biogenic magnetic nanoparticles biomineralized by magnetotactic bacteria. For instance, the alphaproteobacterium

*Magnetospirillum gryphiswaldense* synthesizes up to 40 intracellular nanocrystals of chemically pure magnetite (Fe<sub>3</sub>O<sub>4</sub>) that are surrounded by a phospholipid bilayer (Figure 1).<sup>[7,8]</sup> The latter not only harbors a set of magnetosome-specific proteins functional in magnetite biomineralization,<sup>[9–11]</sup> but also provides colloidal stability, i.e., after isolation and purification from disrupted cells the particles are stable in aqueous suspensions at a wide range of conditions<sup>[12]</sup>—a prerequisite for potential magnetosome-based applications. Due to a genetically strictly controlled biomineralization process,<sup>[8,10]</sup> cuboctahedral magnetic single-domain nanocrystals are synthesized that exhibit extraordinary material properties such as a strong magnetization, high crystallinity, and a narrow particle size distribution that can hardly be achieved by chemical synthesis.<sup>[13–16]</sup> However, potential magnetosome-based applications require the long-term storage of the particles, and little is known whether the nanoparticles can be stored for prolonged time periods without quality deficits.

Sodium azide or other aseptics have commonly been used to prevent microbial contaminations; however, such a treatment restricts potential applications of magnetosomes to in vitro environments.<sup>[17]</sup> Although magnetosomes can be stored frozen at –20 °C or –80 °C, in particular for functionalized, e.g. enzyme displaying particles, a significantly diminished catalytic activity was observed upon freezing and thawing. Thus, after three or five freeze-thaw cycles the tested functionalized magnetosomes lost up to 72% of their activity, suggesting protein denaturation and loss of membrane integrity.<sup>[18]</sup>

To ensure long-term stability, magnetosomes as well as chemically synthesized nanoparticles can be autoclaved (which, however, causes loss of biological activity) and/or irradiated.

F. Mickoleit, S. Markert, D. Schüler  
Department of Microbiology  
University of Bayreuth  
Universitätsstraße 30, D-95447 Bayreuth, Germany  
E-mail: dirk.schueler@uni-bayreuth.de


C. Jörke, J. H. Clement  
Department of Hematology and Medical Oncology  
Jena University Hospital  
Am Klinikum 1, D-07747 Jena, Germany  
E-mail: joachim.clement@med.uni-jena.de

R. Richter, I. Rehberg, O. Bäumchen  
Experimental Physics V  
University of Bayreuth  
Universitätsstraße 30, D-95447 Bayreuth, Germany

S. Rosenfeldt, A. S. Schenk  
Bavarian Polymer Institute (BPI)  
University of Bayreuth  
Universitätsstraße 30, D-95447 Bayreuth, Germany

S. Rosenfeldt  
Physical Chemistry I  
University of Bayreuth  
Universitätsstraße 30, D-95447 Bayreuth, Germany

A. S. Schenk  
Physical Chemistry IV  
University of Bayreuth  
Universitätsstraße 30, D-95447 Bayreuth, Germany

 The ORCID identification number(s) for the author(s) of this article can be found under <https://doi.org/10.1002/sml.202206244>.

© 2023 The Authors. Small published by Wiley-VCH GmbH. This is an open access article under the terms of the Creative Commons Attribution License, which permits use, distribution and reproduction in any medium, provided the original work is properly cited.

DOI: 10.1002/sml.202206244

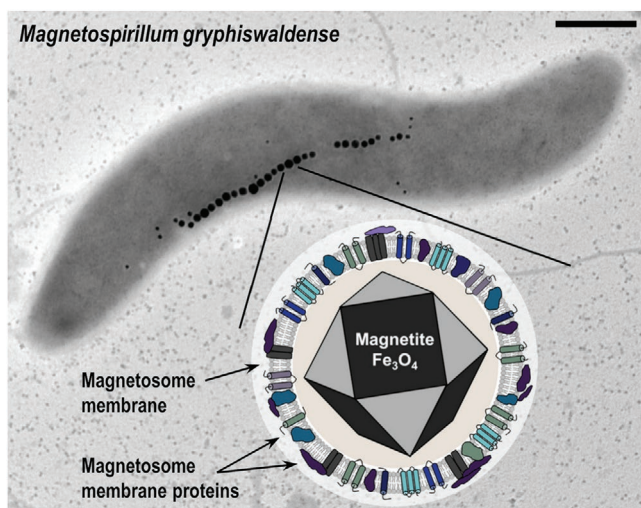


**Figure 1.** Magnetosome formation in *M. gryphiswaldense*. Under micro-oxic/anoxic cultivation conditions, the wild-type strain biomineralizes up to 40 magnetosomes, which are arranged in a chain-like manner at midcell. The particles consist of a cuboctahedral magnetite core that is surrounded by a proteinaceous phospholipid bilayer (magnetosome membrane). The latter harbors a set of magnetosome-specific proteins, which are functional in magnetite biomineralization. Scale bar 0.5  $\mu\text{m}$ .

Partially, these treatments are combined with an initial filtration step. Furthermore, combinations of lyophilization and irradiation were investigated to enable reliable in vivo applications of magnetosomes.<sup>[19–23]</sup>

Although these routes allow the storage under sterile conditions, effects on the nanoparticles' characteristics cannot be excluded. Furthermore, pretreatment also depends on the specific application and has to be validated case-by-case. Thereby, it has to be ensured that the chosen technique retains the magnetosome properties, in particular the particle morphology and the integrity of the magnetosome membrane as well as further surface modifications (such as surface-exposed functionalities). Due to these constraints, in many cell culture studies only freshly purified magnetosomes were tested.<sup>[24,25]</sup>

The biocompatibility of isolated magnetosomes and their interaction with mammalian cell lines has been investigated in a variety of studies.<sup>[14,24,26]</sup> Recently, our group evaluated the uptake and intracellular localization of magnetosomes by FaDu hypopharynx carcinoma cells, and assessed the viability and cell death rates for different cancer cell lines as well as primary cells when incubated with increasing particle amounts.<sup>[12,27]</sup> From these studies magnetosomes were considered to be biocompatible. Even for the highest tested magnetosome concentration (100  $\mu\text{g cm}^{-2}$ ) viability values in the range from 70 to 80% were obtained after 48 h of incubation.

However, the particles' (colloidal) stability and biocompatibility upon long-term storage have so far not been fully addressed, and no long-range investigations are available. This is of eminent importance for future biomedical and clinical applications of magnetosomes. Therefore, in this study, we monitored the properties of a batch of magnetosomes at monthly intervals without applying any autoclaving, lyophilization, or further sterilization techniques to the magnetosomes. Based on the definition for the stability of (chemically synthe-

sized) nanoparticles by Phan and Haes,<sup>[28]</sup> we thereby investigated the magnetosome suspensions with regard to different criteria such as the particles' morphology, their uniformity and size distribution, the colloidal stability, their magnetization as well as their surface properties, in particular the surface charge and the integrity of the surrounding magnetosome membrane.

## 2. Results

### 2.1. Freshly Isolated Magnetosome Suspensions Contain Well-Dispersed Particles with Intact Membranes

Magnetosomes were isolated from microoxically cultivated wild-type (WT) cells of *M. gryphiswaldense* and purified according to established procedures.<sup>[27,29]</sup> The particles were resuspended in 10 mM HEPES/1 mM EDTA, pH 7.2, which has proven to ensure colloidal stability,<sup>[12]</sup> and afterwards fractionated into 12 identical aliquots. The latter were stored at 4 °C under a nitrogen atmosphere until the respective measurements were performed. Each month, one aliquot was analyzed with regard to particle morphology, i.e., the integrity of the magnetite core and magnetosome membrane, surface charge, colloidal stability, and the formation of particle agglomerates, as well as biocompatibility. Initial investigations were conducted on the freshly prepared suspension (denoted in the following as aliquot “Month 1”), which was followed by further consecutive, monthly performed analyses (aliquots “Month 2–12”), thereby providing a comprehensive overview of the magnetosome stability for a storage time of almost one year.

As indicated by transmission electron microscopy (TEM) images, the freshly isolated magnetosome suspension was free of impurities and contained well-dispersed individual particles and smaller agglomerates. The magnetite crystals ( $35.7 \pm 7.2$  nm in diameter; estimated from TEM) were surrounded by an electron-light organic layer of  $\approx 5$  nm thickness, representing the (intact) magnetosome membrane (Figure 2A,B and Figure S1, Supporting Information, “Month 1”). The overall mean particle diameter of  $40.2 \pm 5.7$  nm is in accordance with values previously reported.<sup>[7,12,27]</sup> Characterization of a concentrated particle suspension by small angle X-ray scattering (SAXS) revealed a crystal size of  $37 \pm 6$  nm assuming a Gaussian size distribution and a mean magnetosome–magnetosome distance of  $d = 47$  nm (Figure S2, Supporting Information, Table 1).

The tendency of single magnetosomes to form smaller agglomerates was reflected by dynamic light scattering (DLS) measurements (Table S1, Supporting Information). Here, due to the formation of a hydration shell, particle diameters were slightly increased compared to values determined by TEM. Volume-weighted size distributions revealed the presence of different particle size “classes”. For the freshly isolated particle suspension, hydrodynamic diameters of  $41.1 \pm 11.2$  and  $99.3 \pm 23.7$  nm may be ascribed to single magnetosomes and smaller clusters, whereas overall sizes of  $151.7 \pm 8.0$  nm are most likely related to agglomerates or magnetosome chains. Please note that the applied volume-averaging technique is based on the hydrodynamic radius of spherical objects. In absorption-based sedimentation assays of diluted magnetosome suspensions (0.10 mg Fe mL<sup>-1</sup>) a slow, gradual clarification and

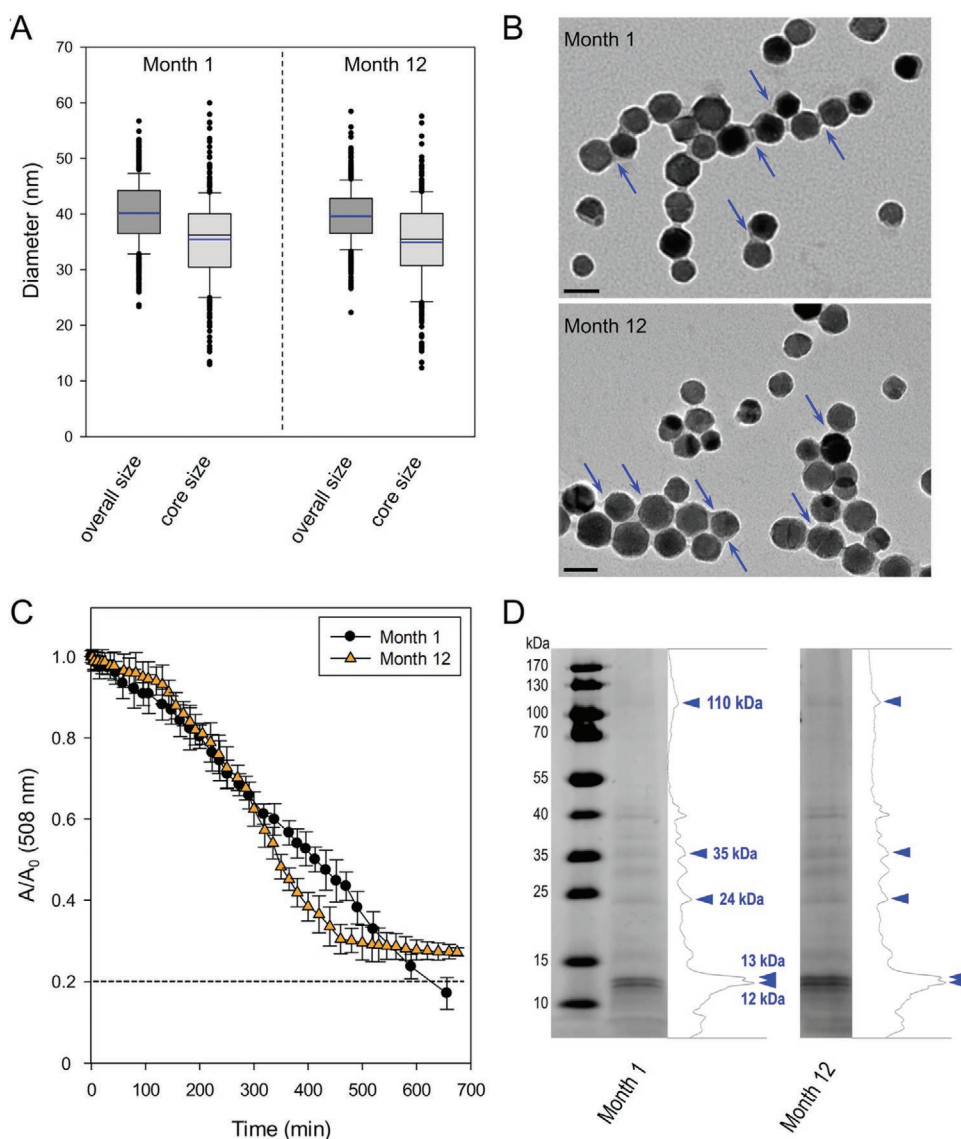


**Figure 2.** Size distribution, morphology, and (colloidal) stability of purified magnetosomes upon long-term storage. A) Box plot illustrating the respective particle size distribution (measured from TEM micrographs), i.e., the overall diameter and the size of the crystal core at different time points (freshly isolated, “Month 1” and stored suspensions, “Month 12”),  $n > 350$ . The boundary of each box closest to zero indicates the 25th percentile, a black line within the boxes marks the median, and the boundary of the boxes farthest from zero indicates the 75th percentile (50% central data). Whiskers above and below the boxes represent the 90th and 10th percentiles, and blue lines indicate the mean values. Data that lie outside the 10th and 90th percentile are plotted as black dots. For “Month 1” and “Month 12” similar particle size distributions were observed, with no statistically significant differences. B) TEM micrographs revealed the presence of single magnetosomes as well as smaller particle agglomerates in both samples. Furthermore, identical particle morphologies were observed, with the magnetite cores being surrounded by an electron-light organic shell (indicated by blue arrows) representing the magnetosome membrane. Scale bar 50 nm. C) In time-dependent sedimentation assays of diluted magnetosome suspensions (each  $0.10 \text{ mg Fe mL}^{-1}$ ), for “Month 1” and “Month 12” similar profiles were obtained. An absorption ratio  $A/A_0$  of 20% is indicated by a dashed line. D) SDS-PAGE analyses of the solubilized magnetosome membrane fraction revealed similar banding patterns for “Month 1” and “Month 12”, suggesting integrity of the magnetosome membrane and its embedded proteins after long-term storage. Five protein bands are highlighted (blue arrows) to facilitate direct comparison of the protein banding profiles. Furthermore, for the respective lanes the densitometric profiles are provided, illustrating comparable band intensities. Protein molecular weight marker, ThermoScientific PageRuler prestained protein ladder.

the formation of a dark-brownish pellet was observed, with less than 20% of the particles being in the supernatant after  $\approx 11 \text{ h}$  (Figure 2C, Figure S3, Supporting Information). These tendencies of the particles to settle down might again be ascribed to the formation of magnetosome agglomerates, or a (partial) loss of colloidal stability due to insufficient stabilization of the mag-

netite crystals (for example as a consequence of magnetosome membrane rupture). However, the pellet could be readily resuspended by inverting the cuvette, which argues for largely intact magnetosome membranes.

The presence of the magnetosome membrane as a surrounding, proteinaceous phospholipid bilayer caused a negative

**Table 1.** Comparison of the values obtained from a fit of the magnetization curve and other sources. For more details, please refer to the text.

Magnetosome sample	Saturation magnetization $M_s$ [ $A\ m^{-1}$ ]	Dipole moment $m_1$ [ $aA\ m^2$ ]	Number density $n_f$ ( $\frac{10^{10}}{mm^3}$ )	Magnetic core diameter $d_m$ [nm]	Extended particle diameter $d'_m = d_m + d_{dead}$ [nm]	Crystal diameter from TEM images $d_{TEM}$ [nm]	Overall diameter from TEM images $d_{all}$ [nm]	Crystal diameter SAXS [nm]
From freshly isolated batch	80.8	5.2	1.55	34.7	36.1	$35.7 \pm 7.2$	$40.2 \pm 5.7$	$37 \pm 6$
Stored/aged ("Month 12")	26.6	2.4	1.11	26.3	27.7	$34.8 \pm 7.6$	$39.6 \pm 5.1$	$37 \pm 6$
Ratio 1st/2nd	3.04	2.2	1.4	1.32	1.3	1.02	1.02	1.0

particle surface charge, as indicated by a zeta potential of  $-35.8 \pm 3.4$  mV (determined in 10 mM HEPES/1 mM EDTA, pH 7.2). This value is in accordance with previous analyses, in which zeta potentials ranging from  $-34$  to  $-38$  mV were measured.<sup>[30–32]</sup> As a proxy for the integrity of the surrounding magnetosome membrane, we subjected solubilized magnetosome samples to denaturing polyacrylamide gel electrophoresis (PAGE), followed by Coomassie blue staining of the gel. Thereby, a protein banding pattern was obtained (Figure 2D) that resembled previous PAGE analyses.<sup>[9,31]</sup> Characteristic predominant bands that were previously identified as MamF (molecular mass of 12 and 110 kDa as calculated from electrophoretic mobility), MamC (13 kDa), MamA (24 kDa) and MamM (35 kDa)<sup>[9]</sup> (Figure 2D, Figure S4, Supporting Information; indicated by blue arrows) were chosen as tracers for the integrity of the membrane proteins in the monthly performed PAGE analysis.

MamC and MamF are highly abundant, integral membrane proteins with two or three transmembrane helices. Their abundances were estimated to be within the range of 80–100 (MamC) or 60–80 (MamF) copies per particle.<sup>[9,11,33]</sup> Both proteins have redundant functions and play only accessory roles in magnetite biomineralization (control of size and shape), as in the respective deletion strains particles with only slightly reduced diameters were produced, and a tendency to spontaneously self-assemble has been reported.<sup>[7,8,34]</sup> The membrane-associated MamA is present in a similar copy number as MamC (approximately 85 copies<sup>[33]</sup>) and is supposed to assist the recruitment of other magnetosome proteins to the membrane. However, deletion of *mamA* does not have any effect on magnetosome biosynthesis, ascribing MamA an only nonessential function.<sup>[35]</sup> For the essential integral MamM protein, a role in iron transport has been suggested as well as an involvement in crystallization initiation and proper localization of other magnetosome proteins. Thus, *mamM* deletion results in the formation of empty magnetosome vesicles and loss of magnetite crystal formation.<sup>[36]</sup>

## 2.2. Particle Morphology, Colloidal Stability and Membrane Integrity Are Not Affected upon Long-Term Storage

During storage, only slight variations in the monitored parameters were observed. Re-evaluation of the magnetosomes size at timepoint 12 ("Month 12") revealed a magnetite core size of  $34.8 \pm 7.6$  nm and an overall particle diameter of  $39.6 \pm 5.1$  nm (Figure 2A, TEM analysis). Using SAXS analysis, again a

crystal size of  $37 \pm 6$  nm (assuming a Gaussian size distribution) and a mean distance of approx. 63 nm for neighboring magnetosomes were obtained (Figure S2, Supporting Information, Table 1). As expected, the size of the crystal did not change with time. However, no information on the iron oxide species can be obtained by this method. Since the preparation of the samples is identical, the observed difference in the distance of neighboring magnetosomes may hint to slightly different interparticle interactions in the aged sample ("Month 12") compared to the freshly prepared one. Possible explanations are slightly different particle densities, the partial oxidation of the magnetite crystals, or different stabilization capacities of the magnetosome membrane.

For the sample "Month 12", the hydrodynamic diameter of  $82.0 \pm 37.2$  nm measured by DLS might again represent single magnetosome particles, whereas sizes of  $404.5 \pm 126.5$  nm and  $856.6 \pm 283.5$  nm may indicate the presence of particle agglomerates, chains, or combinations thereof. The distinct particle size "classes" provided by DLS for the different monthly-analyzed samples are given in Table S1. The respective sedimentation profiles for timepoints "Month 1" and "Month 2" were nearly identical, however, for the following months 3–12, slight changes were detected. Thus, in the absorption-based assays sedimentation rates significantly increased after 300 min. Despite these accelerated tendencies of the particles to settle down, sedimentation was stabilized to  $\approx 30\%$  after 500–600 min (Figure 2C, Figure S3, Supporting Information), suggesting that a distinct portion of the particles remained stable in suspension.

The protein banding patterns on SDS gels obtained by denaturing PAGE showed no obvious aberrations, disregarding slight differences in the migration behavior of the individual magnetosome membrane proteins potentially caused by the gel preparation (Figure 2D, Figure S4, Supporting Information). The chosen tracer protein bands were present on each monthly prepared SDS-gel (Figure S4, Supporting Information), and their relative intensities varied only marginally. Accordingly, the designated MamF bands constituted 11–15% (12 kDa) and 3–4% (110 kDa) to the overall lane intensity as determined by densitometric analyses. For MamC, MamA, and MamM relative band intensities of 11–15%, 6–7%, and 5–6%, respectively, were calculated. Although it cannot be completely excluded that magnetosome proteins were released from the membrane, these values indicate that the long-term storage at the chosen conditions (i.e., at 4 °C under a nitrogen atmosphere) did not lead to any obvious protein degradation. In addition, no significant changes regarding the surface charge were observed during storage (Table S1, Supporting Information).

As many envisioned applications of magnetosomes would benefit from particles that display further functionalities,<sup>[25,37]</sup> we investigated whether the magnetosome membrane is still able to bind further molecules on its surface. For this purpose, freshly isolated magnetosomes (month 1) as well as stored particles (month 12) were fluorescently labeled in a chemical crosslinking reaction using DyLight 488 NHS ester. After the removal of unbound/excess dye by extensive washing, fluorescence measurements (535 nm) revealed comparable signal intensities (Figure S5, Supporting Information), indicating similar labelling efficiencies even after long-term storage. For unlabeled magnetosomes, which were taken as control, only low background signals were observed.

Thus, taken together, these results suggest that the magnetosome membrane remained largely intact, and still provides colloidal stability as well as sites for chemical attachment of functional moieties, even after storage for almost one year. However, it still had to be elucidated whether this intact membrane also safeguards the magnetic properties of the magnetosomes.

### 2.3. Magnetization Curves Show a Decay of the Magnetic Potency upon Storage

Magnetization curves of different magnetosome suspensions were measured by means of a vibrating sample magnetometer (VSM).<sup>[38]</sup> For details refer to the Experimental Section and Figure S6 (Supporting Information). **Figure 3A** shows the magnetization curves of a fresh (red squares) and an aged sample (purple circles) versus the effective magnetic induction  $B_e$ .<sup>[39]</sup> Following Rehberg et al.<sup>[39]</sup> we fit the experimental data by a superposition of Langevin functions

$$M(B_e) = \sum_{k=1}^l M_k L\left(\frac{m_k B_e}{k_B T}\right) \quad (1)$$

Here  $M_k$  denotes the saturation magnetization of the  $k^{\text{th}}$  fraction, with the dipole moment  $m_k$ , the Boltzmann constant  $k_B$ , the absolute temperature  $T$ , and the Langevin function

$$L(\alpha) = \coth(\alpha) - \frac{1}{\alpha} \quad (2)$$

The two solid lines in Figure 3A denote the best fits of the experimental data to Equation (1). Both samples are well described with  $l = 1$ , i.e., a monodisperse ansatz, an indication for the narrow size distribution of magnetosomes in the suspensions. In contrast, for commercial ferrofluids, one typically needs  $l = 4$ .<sup>[39]</sup> The similarity of both curves is demonstrated in the inset, where the  $B_e$ -axis is scaled by the characteristic field  $B_c = \frac{k_B T}{m}$ , and the magnetization  $M$  by the saturation magnetization  $M_s$ . Both data fall onto the resulting master curve (green line).

A list of all fitting results is presented in Table 1. The first column indicates that the aged sample (“Month 12”) has about one third of the saturation magnetization  $M_s$  of the freshly isolated sample. The second column shows that the prominent dipole moment  $m_1$  is diminished by about one half. With the simplest assumption of a fixed decay constant  $\frac{dm}{dt} \frac{1}{m}$ , i.e., we suppose that the decay rate of the magnetic moment is

proportional to the moment of not yet decayed material, one yields an exponential decay with a lifetime of about 470 d. The third column indicates that the number density  $n_1 = \frac{m_1}{M_1}$  is slightly reduced during one year.

The dipole moment  $m$  of a magnetosome allows for an estimate of its volume by  $V = \frac{m}{M_d}$ , using the saturation magnetization of a one-domain particle of magnetite of  $M_d = 464 \frac{kA}{m}$ .<sup>[40]</sup> Taking into account that the magnetosomes are cuboctahedra, we obtain the diameter of the circumscribed sphere as  $d_m = 2\left(\frac{3}{5\sqrt{2}}V\right)^{1/3}$ . The resulting values are presented as “magnetic core diameter” for the freshly isolated and for the aged sample. They can be compared with  $d_{\text{TEM}}$  as measured from TEM images and presented in Figure 2A.

A more sensitive comparison is provided by the extended particle diameter  $d'_m$  in Table 1. It considers the core-shell configuration of magnetic nanoparticles, i.e., a core with ferromagnetically ordered spins is surrounded by a spin-disordered shell, which is known as magnetic dead layer.<sup>[41–43]</sup> For magnetite, the thickness of the dead layer is  $d_{\text{dead}} \approx 0.7$  nm,<sup>[44]</sup> which we add according to  $d'_m = d_m + 2 d_{\text{dead}}$ . For the freshly isolated sample  $d'_m$  differs by only 0.5 nm from  $d_{\text{TEM}}$  and is situated well within the error bars. However, for the aged sample  $d'_m$  is 7.2 nm smaller than  $d_{\text{TEM}}$ . This indicates that over a period of one year the magnetic active diameter of the magnetosomes became considerably diminished by about a factor of 0.76. A potential explanation might be the oxidation of magnetite via maghemite  $\left(M_d = 378 \frac{kA}{m}\right)$  to hematite  $\left(M_d = 2 \frac{kA}{m}\right)$ , despite the surrounding magnetosome membrane. However, in spite of the observed reduced saturation magnetization after long-term storage, it should be emphasized that the particles are still magnetic and can be attracted in a magnetic field gradient—which is an important prerequisite for envisioned magnetosome-based applications.

In order to corroborate this conjecture, we have further studied the aged sample. After removing the sample from its protected storage (4 °C, nitrogen atmosphere) and filling it into the sample holder, the M(H)-curve was measured seven times within 100 h. Figure 3B displays the saturation magnetization  $M_s$ , which decays with time. In a first approximation, we assume a fixed decay constant  $\lambda = \frac{dM_s}{dt} \frac{1}{M_s}$ , which is obtained from an exponential fit (as marked by the black solid line) yielding a lifetime of  $\tau = \lambda^{-1} \approx 45.3$  d. This lifetime is about ten times shorter than the one estimated for one year under ideal storing conditions. Assuming that potential oxidative effects might diminish the saturation magnetization of the particle suspension to some extent, a likely oxidation during measurement may be faster than during storage under nitrogen atmosphere and reduced temperature, because a plain thread—which is not leak tight against oxygen—closes the sample holder of the VSM.

Combining the results from VMS, DLS, and SAXS, we hypothesize that even if the magnetosomes are stored at 4 °C under an inert gas atmosphere, partial oxidation of the magnetite crystal cannot be fully prevented. Most probably, a slight morphological

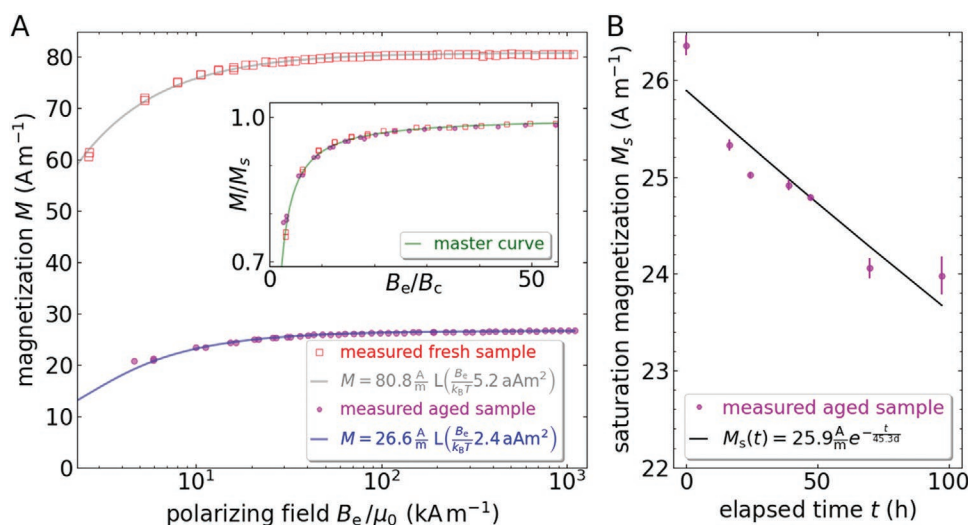


**Figure 3.** Magnetization of different magnetosome suspensions. A) Magnetization versus the effective polarizing field. The symbols mark the experimentally measured values, the solid lines represent the best fits by Equation (1). For clarity, only every 16<sup>th</sup> experimental value is plotted. In the inset, the  $B_e$ -axis is scaled by the characteristic field  $B_c = \frac{k_B T}{m}$ , and the magnetization  $M$  by the saturation magnetization  $M_s$ . B)  $M_s$  of the aged sample (“Month 12”) versus the elapsed time after filling the sample (obtained from the fridge) into the sample holder. The solid black line marks the fit yielding a lifetime of 45.3 d. The error bars denote the standard deviation of the measured data from the fitted curve for polarizing fields larger than 200 kAm<sup>-1</sup>.

restructuring of the magnetosome shell is introduced by the storage conditions, allowing for a better oxygen penetration, thereby resulting in a change in the surface interaction potential and an increasing tendency to form agglomerates. Further studies should therefore investigate if the crystal will suffer all-over oxidation or if oxidation may stop at a certain passivation layer.

## 2.4. Biocompatibility Studies on Stored Magnetosome Suspensions

In order to evaluate potential cytotoxic effects deriving from the magnetosome suspensions, we used two mammalian cell lines, the adherent squamous hypopharynx carcinoma cell line FaDu and the adherent non-small cell lung carcinoma cell line HCC78. As previously reported, magnetosomes exhibit a good biocompatibility towards these cell lines.<sup>[12,27]</sup> Both cell lines were incubated with different magnetosome concentrations (i.e., 5, 25, 50, and 100  $\mu\text{g Fe cm}^{-2}$ , corresponding to 19.4, 97.2, 194.4 and 388.9  $\mu\text{g Fe mL}^{-1}$ , respectively) for 24 or 48 h. Experiments were performed monthly applying the respective, stored magnetosome suspensions, and cell viability was assessed by using PrestoBlue assays. Untreated cells and cells incubated with HEPES buffer served as negative control, cells treated with Triton X-100 were taken as positive control. For the FaDu cell line concentration-dependent effects on the cell viability were observed (Figure 4A,B), with the highest tested particle concentration of 100  $\mu\text{g Fe cm}^{-2}$  reducing the overall cell viability (i.e., averaged over 12 months) to 73.8% (24 h) or 73.9% (48 h). However, these values still confirm good to moderate biocompatibility (classified according to EN ISO 10993-5:2009<sup>[45]</sup>). Similar albeit more pronounced effects were observed for the more sensitive HCC78 cell line (Figure 4C,D). Here, for an incubation time of 24 or 48 h and a magnetosome amount of 100  $\mu\text{g Fe cm}^{-2}$  the overall cell viability was decreased to 75.7% or 63.1%, respectively.

During long-term storage, for both cell lines minor fluctuations of the cell viability rates were observed (Figures S7 and S8, Supporting Information). Although for some time points and magnetosome concentrations viability values <60% were measured (in particular for the HCC78 cell line after 48 h incubation applying magnetosome suspensions stored for longer than eight months; Figure S8, Supporting Information), particle amounts of up to 50  $\mu\text{g Fe cm}^{-2}$  are considered to be biocompatible. Thus, for the FaDu and HCC78 cell lines average viability values of 67 (57-73; month 12: 71)% (FaDu) and 79 (39-96; month 12: 71)% (HCC78) were determined for 50  $\mu\text{g Fe cm}^{-2}$  and 24 h of incubation. After 48 h, viability remained in this range with 73 (67-91; month 12: 67)% (FaDu) and 73 (36-90; month 12: 58)% (HCC78). These values indicate that the particles can be safely administered even after storage for almost one year.

PrestoBlue viability data could be confirmed by (semi-)quantitative determination of cell death rates using SYTOX staining followed by flow cytometric analyses, thereby collecting data on the total number of vital cells (Figure S9, Supporting Information). For that purpose, the FaDu or HCC78 cell line (each 500 000 cells) was incubated with different magnetosome concentrations (5, 25, or 100  $\mu\text{g Fe cm}^{-2}$ ) for 24 h (“Month 1”) or 24 and 48 h (“Month 12”). Obtained values were finally taken to calculate cell viability rates, with untreated cells or cells treated with 0.1% Triton X-100 serving as controls. For both the freshly isolated magnetosomes (“Month 1”) as well as the stored particle suspensions (“Month 12”) similar cell viability values were determined. While in the presence of Triton X-100 without magnetosomes cell viability was drastically reduced (16% for FaDu and 42% for HCC78), the magnetosome-treated samples were unaffected and viability values were comparable to the respective untreated controls ( $\geq 85\%$ ) for all concentrations and incubation times.

Overall, as concluded from our physicochemical analyses, the viability data suggest the presence of intact particles with

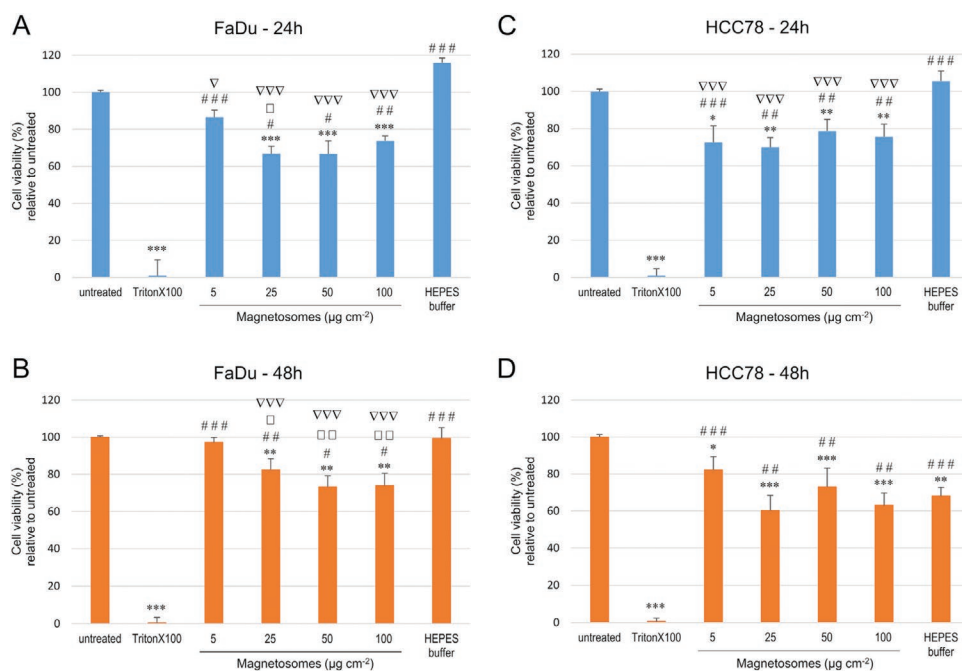


**Figure 4.** Effect of magnetosomes on cell viability. The cell lines FaDu (A,B) and HCC78 (C,D) were incubated with 5, 25, 50, or 100  $\mu\text{g cm}^{-2}$  magnetosomes for 24 h (blue bars) and 48 h (orange bars). With the PrestoBlue reagent, the viability of the cell cultures was determined. The figures are a compilation of the results from the monthly performed measurements (month 1–12). Viability values are given as percentage relative to the untreated fraction (negative control). Cells incubated with 0.1% Triton X-100 served as positive control. Statistically significant differences are denoted as follows:  $p < 0.05$  (\*; #; □; ∇),  $p < 0.01$  (\*\*; ##; □□; ∇∇),  $p < 0.001$  (\*\*\*; ###; □□□; ∇∇∇). Statistical analysis and  $p$ -values are provided in Table S3 (Supporting Information).

regard to membrane integrity and no obvious degradation effects that might cause increased cytotoxic effects. Hence, the hypothesized partial oxidation of the magnetite crystal appears to play only a minor role in cytotoxicity, if any.

### 3. Discussion

The stability of artificial magnetic nanoparticles has been investigated in many studies.<sup>[5,20,46]</sup> Conditioned by their synthesis, additional coatings with various shells such as chemical/biological membranes, gold, or polymeric matrixes have to be applied as the “naked” particles usually lack colloidal stability and exhibit partially high toxicity.<sup>[1,47–50]</sup> In contrast, bacterial magnetosomes are naturally enveloped by a protein-rich phospholipid bilayer that not only stabilizes the particles but is also supposed to reduce the oxidation of the magnetite crystals to some extent.<sup>[13,51]</sup> Furthermore, it provides biocompatibility and significantly reduces cytotoxic effects when administered to eukaryotic cells.<sup>[52,53]</sup> Thus, integrity and preservation of the magnetosome membrane during prolonged storage of the particle suspensions might be crucial for their application potential. However, the long-term stability of isolated magnetosomes has so far not been fully assessed. Instead, for (prolonged) storage and application in cell culture or in vivo studies the particles were usually sterilized by autoclaving<sup>[21,54]</sup> or irradiation (e.g., gamma-rays or  $\text{Co}_60$ ).<sup>[22,55–57]</sup>

In our study, we demonstrate that isolated magnetosomes can be stored as aqueous, buffered suspensions under a nitrogen atmosphere at 4 °C without further post-treatments or the addition of antibiotics. As for a high fraction the colloidal

stability, the surface charge, and the protein banding patterns of the solubilized magnetosome membranes remain unaffected, the particles are sufficiently stable even after storage for almost one year. It thus can be assumed that the surrounding magnetosome membrane is not basically affected by long-term storage at the applied conditions. Measuring the magnetization curves of a freshly prepared suspension of magnetosomes and that of one aged for 12 months under storage conditions (4 °C, nitrogen atmosphere), the long-term stability of the magnetic properties was tested. Over this period of time the saturation magnetization dropped to one-third of its initial value. Follow-up measurements of the aged sample for four days unveiled a ten times shorter lifetime of the normalized saturation magnetization under less optimal conditions (i.e., atmosphere and room temperature). One may hypothesize, that even an intact magnetosome membrane cannot fully prevent partial oxidation of the magnetite. This agrees with the results reported by Fischer et al.<sup>[58]</sup> They demonstrated by means of synchrotron X-ray diffraction that intracellular magnetite is pure, whereas isolated magnetosomes become partially oxidized. This suggests that the bacteria generate optimal physicochemical conditions for the stability of magnetite.

In comparison to standard ferrofluids, which have a particle diameter of around 10 nm, magnetosomes are large, with a diameter of around 40 nm. Thus, our suspensions have an enhanced magnetic coupling parameter (see Mickoleit et al.<sup>[59]</sup>) and should be prone to agglomeration and sedimentation. This is even accelerated in magnetic fields. Indeed, sedimentation takes place during long-term (7 h) measurements of the magnetization curve, but is reversible. This agglomeration can be neglected by restricting the measuring time to 2 h. Under these

conditions the magnetic core diameter, as determined from the magnetization curve, meets very well the diameter determined from TEM micrographs for fresh particles. In addition, the analysis of the magnetization curves allows to monitor a decay of the magnetic potency. The magnetization curves of magnetosomes in suspension are thus a valuable supplement to those on solid substrates.<sup>[51]</sup>

Cytotoxicity of bacterial magnetosomes has been investigated on a variety of eukaryotic cell lines. Effects on cell viability mostly depended on both the particle concentration as well as the incubation time. For instance, magnetosomes concentrations of 125  $\mu\text{g mL}^{-1}$  could be safely administered to MDA-MB-231 epithelial, human breast cancer cells with only 3% decrease in cell viability.<sup>[60]</sup> Similarly, the viability of J774 mouse macrophage cells was only slightly affected for particle concentrations ranging from 10 to 140  $\mu\text{g mL}^{-1}$  (more than 90% vital cells after 24 h of incubation).<sup>[61]</sup> In contrast, for chemically synthesized iron oxide nanoparticles, clearly increased cytotoxic effects were observed. Thus, for the J774 cell line particle concentrations of 25–200  $\mu\text{g mL}^{-1}$  reduced cell viability to  $\approx 25\%$ .<sup>[62]</sup> In our study, cytotoxicity of magnetosomes upon long-term storage was assessed on the FaDu and HCC78 cell line. Besides investigations regarding concentration-dependent effects, the monthly collected data were directly compared with each other. Cell viability rates resembled those reported previously for freshly isolated magnetosome preparations.<sup>[12,27]</sup> For the robust FaDu cell line the overall cell viability averaged over 12 months slightly decreased with increasing magnetosome amounts (as indicated from PrestoBlue assays). This effect was even more pronounced for 48 h of incubation. However, for the highest tested concentration (100  $\mu\text{g cm}^{-2} \triangleq 388.9 \mu\text{g Fe mL}^{-1}$ ) still average viability values  $\geq 73\%$  were determined, classifying magnetosomes as biocompatible.<sup>[45]</sup> Cytotoxicity testing on the more sensitive HCC78 cell line revealed viability values of 63% to 82%, with visible concentration-dependent effects after 48 h. Overall, in the course of our monthly performed analyses similar, reproducible viability values were determined for both cell lines. These data suggest that biocompatibility is not severely affected upon long-term storage, and particle concentrations up to 50  $\mu\text{g cm}^{-2}$  are considered to be biocompatible regardless their storage time. For the magnetosome subfractions stored for different time periods, similar cell–particle interactions can be assumed, since physicochemical analyses indicated no obvious changes in the colloidal stability and the presence of a still intact surrounding magnetosome membrane. The latter preserves the inherent characteristics of the particles, leading to a consistently low cytotoxicity and comparable particle availability in the incubation assays.

## 4. Conclusion

In our study, we assessed the stability and biocompatibility of isolated magnetosomes during long-term storage for almost one year. Thereby we followed a recent study by Phan and Haes who suggested different criteria for the stability of chemically synthesized nanoparticles.<sup>[28]</sup> Our analyses demonstrate that magnetosomes can be safely stored as an aqueous suspension. The particles' morphology, the integrity of the magnetosome

membrane, their colloidal stability, and the biocompatibility of the particle suspensions remain stable. However, lacking their protective environment within the cells, the magnetic potency of the particles decays, as indicated by magnetization curves. This is presumably caused by oxidative processes of the magnetite crystals. The lifetime of the magnetosome suspension is prolonged by a factor of ten under the presented storage conditions and amounts to 470 d. Overall, our study clearly strengthens and enhances the potential of magnetosomes for biomedical and future clinical applications by defining crucial quality parameters. As the particles are easy to handle and can be readily stored for prolonged time periods, they provide a promising alternative to chemically synthesized nanoparticle formulations.

## 5. Experimental Section

**Cultivation of *M. gryphiswaldense* and Magnetosome Isolation:** The wild-type strain of *M. gryphiswaldense*<sup>[63,64]</sup> was grown in a modified flask standard medium (FSM) as previously described.<sup>[65]</sup> Magnetosomes were isolated from disrupted cells by a two-step purification procedure consisting of magnetic separation and a sucrose high-density ultracentrifugation step as reported previously.<sup>[27,29]</sup> For more details, please refer to the Supplementary Methods (Supporting Information).

**Determination of Iron Concentrations:** The iron content of isolated magnetosome suspensions was determined by atomic absorption spectroscopy (AAS). Sample volumes of 25–50  $\mu\text{L}$  were mixed with 69% nitric acid (final volume 1 mL) and incubated for 3 h at 98 °C. Afterward, the samples were filled up with ddH<sub>2</sub>O to a final volume of 3 mL and analyzed using a contrAA 300 high-resolution atomic absorption spectrometer (Analytik Jena, Jena, Germany) equipped with a 300 W xenon short-arc lamp (XBO 301, GLE, Berlin, Germany) as the continuum radiation source. The equipment presented a compact high-resolution double monochromator (consisting of a prism pre-monochromator and an echelle grating monochromator) and a charge-coupled device (CCD) array detector with a resolution of about 2 pm per pixel in the far ultraviolet range. An oxidizing air/acetylene flame was used to analyze the samples (wavelength 248.3 nm). The number of pixels of the array detector used for detection was 3 (central pixel 1). Measurements were performed in quintuplicates ( $n = 5$ ), each as a mean of three technical replicates.

**Nanoparticle Sedimentation Assay:** Sedimentation behavior of purified magnetosomes (i.e., the tendency of the particles to settle down) was analyzed as previously described.<sup>[31,66,67]</sup> Briefly, the optical density of a magnetosome suspension (0.10 mg Fe mL<sup>-1</sup>) was measured at a wavelength of 508 nm as a function of time. Absorption values were normalized to the initial absorption measured at  $t = 0$  h (at the beginning of the experiment), thereby allowing direct comparisons between different particle suspensions.

**DLS Measurements:** Zeta potential (ZP) values and particle sizes (i.e., hydrodynamic diameters of single magnetosomes and particle agglomerates) were determined using a Zetasizer Nano-ZS (Malvern, UK). Measurements were performed in the automatic mode at 25 °C on diluted magnetosome suspensions (0.10 mg Fe mL<sup>-1</sup>; in 10 mM HEPES, 1 mM EDTA, pH 7.2). Each sample was analyzed in quintuplicates on three biological replicates ( $n_{\text{total}} = 15$ ) using DTS1070 cuvettes (Malvern, UK). The evaluation software provided by the supplier (Malvern Zetasizer Software 7.13) is based on the Cumulant method and uses the Stokes-Einstein-Equation for size determination. Volume-weighted particle size distributions are used to compare sizes from different samples.

**Magnetic Measurements:** The magnetization curves were measured by means of a vibrating sample magnetometer (VSM) type 7404 from Lake Shore Cryotronics Inc.. For the measurements, the commercially



available sample holder for liquids (Lake Shore Cryotronics Inc., article number 730935) was used, which is made of Kel-F. Its demagnetization factor can be approximated by 0.45.<sup>[38]</sup> In the first step, the dipole moment  $m_0$  of the sample holder filled with plain HEPES buffer was measured for all applied effective fields  $B_e$ . It shows a purely diamagnetic contribution  $m_0$  (as marked in Figure S6, Supporting Information by blue triangles), which is fitted by a linear curve  $m_0(B_e) = a \cdot B_e + B_0$  (indicated in Figure S6, Supporting Information by a red solid line). Thereafter, the sample holder was cleaned with HCl, ddH<sub>2</sub>O, ethanol, and again ddH<sub>2</sub>O. Then, it was filled up to the brim with a magnetosome suspension. The measurement yields then the dipole moment  $m_1$  (cf. Figure S6, Supporting Information, green “+”). The red circles in Figure S6 (Supporting Information) give the effective dipole moment of the magnetosomes, i.e., the outcome of the subtraction  $m = m_1 - m_0$ . The magnetization of the sample was then determined according to  $M = (m_1 - m_0) / V$ , where  $V = 69 \mu\text{L}$  denotes the sample volume.

Two representative magnetization curves are presented in Figure 3A. The upper curve (denoted by open squares) was measured for a freshly prepared suspension of magnetosomes in HEPES buffer. The lower curve (marked by full circles) displays the magnetization of a suspension kept for 12 months under storage conditions (HEPES buffer, 4 °C, nitrogen atmosphere). Those particle suspensions were isolated from the same *M. gryphiswaldense* strain, and prepared and purified in the identical manner with the same iron concentration of 0.10 mg Fe mL<sup>-1</sup>. Because the suspensions are prone to sedimentation (see Figure 2C and Figure S3, Supporting Information) the time for a measurement was intentionally limited to 127.25 min. The integration time was 100 ms. Before each measurement, the sample holder was five times turned upside down and carefully shaken by hand in order to redisperse a possibly settled suspension.

**Small-Angle-X-Ray Scattering (SAXS):** For nano-structural SAXS analyses, magnetosome suspensions in 10 mM HEPES, 1 mM EDTA, pH 7.2 were filled into glass capillaries ( $\varnothing = 1 \text{ mm}$ , code 4007610, Hilgenberg, Germany). The SAXS measurements were performed at ambient conditions using a Double Ganessa AIR system (SAXSLAB/Xenocs). The monochromatic radiation with a wavelength of  $\lambda = 1.54 \text{ \AA}$  is produced by a rotating Cu anode (MicroMax 007HF, Rigaku Corporation, Japan). The position-sensitive detector (PILATUS 300 K, Dectris) was placed at different distances from the sample to cover a wide range of scattering vectors  $q$ , where  $q$  is given as  $q = |\vec{q}| = \frac{4\pi}{\lambda} \sin\left(\frac{\theta}{2}\right)$

with  $\lambda$  representing the wavelength of the incident beam and  $\theta$  the scattering angle. 1D intensity profiles of  $I(q)$  versus  $q$  were obtained by radial averaging. Data were normalized to the intensity of the incident beam, the sample thickness, and the accumulation time. Background correction was performed by subtracting the signal of the diluent-filled capillary. For data analysis the software SasView 4.2. was used.

**Transmission Electron Microscopy (TEM):** For TEM analyses of whole cells or isolated magnetosomes, the respective samples (cell suspensions or highly diluted magnetosome suspensions) were directly deposited onto carbon-coated copper grids (Science Services, Munich, Germany). Magnetosome samples were additionally negatively stained with 2% uranyl acetate. TEM was performed on a JEM-1400Plus transmission electron microscope (JEOL, Tokyo, Japan) operated with an acceleration voltage of 80 kV. Particle sizes were measured from TEM micrographs using the software ImageJ version 1.44p.<sup>[68]</sup>

**Biochemical Methods:** Denaturing polyacrylamide gel electrophoresis (PAGE) was performed according to the method described by Laemmli,<sup>[69]</sup> modified after Fling and Gregerson.<sup>[70]</sup> Gels consisted of a 5% (w/v) acrylamide stacking gel and an 8% → 22.5% (v/w) gradient running gel. Magnetosome suspensions corresponding to 30  $\mu\text{g Fe}$  were incubated in 4× Laemmli sample buffer (325 mM Tris/HCl pH 6.8; 40% glycerol; 400 mM dithiothreitol (DTT); 8% sodium dodecyl sulfate (SDS); 0.01% bromophenol blue) for 10 min at room temperature in order to solubilize magnetosome membrane proteins, which were subsequently separated by electrophoresis.

**Fluorescent Labeling of Isolated Magnetosomes:** Magnetosomes were labeled with a fluorescent dye as previously described.<sup>[12]</sup> Briefly, isolated particles (25  $\mu\text{g Fe}$  in 50 mM NaHCO<sub>3</sub>, pH 9.0) were supplemented with 37.5  $\mu\text{g DyLight 488 NHS ester}$  (Thermo Fisher Scientific, Waltham, MA, USA; stored as a 10 mg mL<sup>-1</sup> stock solution in dimethylformamide) and incubated in the dark for 2 h at 16 °C. After removal of unbound/excess dye by extensive washing, the success of the labeling reaction was confirmed by fluorescence measurements (535 nm) using an Infinite M200pro plate reader (Tecan, Crailsheim, Germany). Fluorescence microscopy analyses were performed using an Olympus IX81 microscope equipped with a Hamamatsu Orca AG camera as described before.<sup>[71]</sup>

**Cell Culture:** For assessing the cytotoxicity of isolated magnetosomes, two mammalian cell lines, the adherent squamous hypopharynx carcinoma cell line FaDu<sup>[72]</sup> and the adherent non-small cell lung carcinoma cell line HCC78<sup>[73]</sup> were used. Both cell lines were cultivated as previously described.<sup>[12]</sup> Detailed description is provided in the Supplementary Methods (Supporting Information).

**PrestoBlue Cytotoxicity Assay:** The effect of various concentrations of magnetosomes on the viability of FaDu and HCC78 cell cultures was analyzed using the PrestoBlue assay (Invitrogen, Karlsruhe, Germany). It is based on the ability of metabolically active, vital cells to reduce the non-fluorescent resazurin to the fluorescent resorufin. For that purpose, 15 000 FaDu or HCC78 cells per well in 72  $\mu\text{L}$  of the respective growth medium supplemented with penicillin/streptomycin (P/S) (10.000 U mL<sup>-1</sup>, 10.000  $\mu\text{g mL}^{-1}$ ) were seeded into a black-walled 96-well plate and cultivated for 24 h. Subsequently, 18  $\mu\text{L}$  magnetosome suspension with final iron concentrations of 5, 25, 50, and 100  $\mu\text{g cm}^{-2}$  (which equals 19.4, 97.2, 194.4, and 388.9  $\mu\text{g Fe mL}^{-1}$ , respectively) diluted with the respective growth medium (supplemented with P/S) were added. For the untreated negative control, 18  $\mu\text{L}$  of the respective growth medium supplemented with P/S was used. As a positive control, 18  $\mu\text{L}$  of Triton X-100 was applied, resulting in a final concentration of 0.02% (w/v). Incubation with the different treatments was performed for 24 or 48 h in a cell culture incubator (37 °C, 5% CO<sub>2</sub>, 95% relative humidity). After incubation, 10  $\mu\text{L}$  of PrestoBlue reagent was added to each well and the plate was incubated for 30 min in a cell culture incubator at 37 °C. Before measuring the plate was placed for 5 additional minutes on a Magnetic-Ring Stand 96-well plate in the dark in order to prevent disturbances by the magnetosomes. The fluorescence intensity (ex/em: 560/600 nm) was measured with the CLARIOstar microplate reader (BMG LABTECH GmbH, Ortenberg, Germany).

**SYTOX Staining:** In order to study cytotoxic effects of magnetosomes, SYTOX staining was performed. SYTOX red dead cell stain (Invitrogen, Karlsruhe, Germany) is a membrane-impermeable DNA dye, which is able to enter cells with compromised cell membranes. When binding to DNA, the dye undergoes significant fluorescence enhancement, leading to a selective staining of dead cells when excited with 633/635 nm red laser light, which can be detected at 658 nm. In scope of evaluating potential cytotoxic effects of magnetosomes, the respective cell lines (FaDu, HCC78; each 500 000 cells) were seeded into 6-well plates and cultivated overnight. After incubation with the indicated concentrations of magnetosomes for 24 or 48 h, the cells including the supernatant were harvested by treatment with Accutase (Sigma-Aldrich, Merck, Darmstadt, Germany). After washing twice with PE (2 mM EDTA in PBS), the cells were resuspended in 500  $\mu\text{L}$  of a 2.5 nM SYTOX red dead cell stain solution and incubated at 4 °C in the dark for 15 min. For control purposes, an unstained sample as well as samples containing only magnetosomes were prepared simultaneously. Furthermore, a positive control using 0.1% Triton X-100 was included. The samples were measured instantly without performing another washing step, because the dye binds in equilibrium with the DNA and therefore external concentration has to be maintained (FACSCalibur, Becton-Dickinson, Heidelberg, Germany).

**Statistical Analyses:** Data are reported as mean  $\pm$  standard deviation. If not otherwise stated,  $n$  represents the number of independent experiments (technical or biological replicates). Sigma Plot software (version 12.0, Systat software Inc., San Jose, CA, USA, 2008) was used

for one-way ANOVA with Holm-Sidak multiple comparisons tests to determine whether data groups significantly differed from each other. Statistical significance was defined either as  $p < 0.05$ ,  $p < 0.01$  or  $p < 0.001$  as specified in the figures and tables.

## Supporting Information

Supporting Information is available from the Wiley Online Library or from the author.

## Acknowledgements

The authors thank Matthias Schlotter (Dept. Microbiology, University of Bayreuth) for technical assistance with cell cultivation and magnetosome isolation. Funding was received in part from the European Research Council (ERC) under the European Union's Horizon 2020 research and innovation program (Grant No. 692637 to D.S.), and from the Federal Ministry of Education and Research (BMBF, grant MagBioFab to D.S.). This project was also funded in part from the Deutsche Forschungsgemeinschaft (DFG), grant CL-202/3-3 (J.H.C.). Further support was received from the Bavarian Academy of Sciences and Humanities (BAW) via a Young Academy fellowship to A.S.S. The authors thank the Bavarian Polymer Institute (BPI) for providing access to the KeyLab "Mesoscale Characterization: Scattering techniques." This work benefited from the use of the SASView application, originally developed under NSF award DMR-0520547. SasView contains code developed with funding from the European Union's Horizon 2020 research and innovation program under SINE2020 project, grant agreement No 654000.

Open access funding enabled and organized by Projekt DEAL.

## Conflict of Interest

The authors declare no conflict of interest.

## Data Availability Statement

Research data are not shared.

## Keywords

biocompatibility, long-term stability, magnetic nanoparticles, magnetization, magnetosomes

Received: October 11, 2022

Revised: January 20, 2023

Published online: February 17, 2023

- [1] E. B. Denkbaş, E. Celik, E. Erdal, D. Kavaz, Ö. Akbal, G. Kara, C. Bayram, in *Nanobiomaterials in Drug Delivery*, (Ed: A. M. Grumezescu), William Andrew Publishing, Norwich, NY **2016**, pp. 285-331.
- [2] J. Mosayebi, M. Kiyasatfar, S. Laurent, *Adv. Healthcare Mater.* **2017**, *6*, 1700306.
- [3] K. El-Boubbou, *Nanomedicine* **2018**, *13*, 953.
- [4] H. V. Tran, N. M. Ngo, R. Medhi, P. Srinoi, T. Liu, S. Rittikulsittichai, T. R. Lee, *Materials* **2022**, *15*, 503.
- [5] A. S. Teja, P. Y. Koh, *Prog. Cryst. Growth Charact. Mater.* **2009**, *55*, 22.
- [6] A. G. Niculescu, C. Chircov, A. M. Grumezescu, *Methods* **2022**, *199*, 16.
- [7] R. Uebe, D. Schüler, *Nat. Rev. Microbiol.* **2016**, *14*, 621.
- [8] D. Schüler, F. D. Müller, in *Bacterial Organelles and Organelle-Like Inclusions*, Vol. 34, (Ed: D. Jendrossek), Springer, Heidelberg, Germany **2020**, pp. 53-70.
- [9] K. Grünberg, E.-C. Müller, A. Otto, R. Reszka, D. Linder, M. Kube, R. Reinhardt, D. Schüler, *Appl. Environ. Microbiol.* **2004**, *70*, 1040.
- [10] A. Lohße, S. Borg, O. Raschdorf, I. Kolinko, É. Tompa, M. Pósfai, D. Faivre, J. Baumgartner, D. Schüler, *J. Bacteriol.* **2014**, *196*, 2658.
- [11] O. Raschdorf, F. Bonn, N. Zeytuni, R. Zarivach, D. Becher, D. Schüler, *J. Proteomics* **2018**, *172*, 89.
- [12] F. Mickoleit, C. Jörke, S. Geimer, D. S. Maier, J. P. Müller, J. Demut, C. Gräfe, D. Schüler, J. H. Clement, *Nanoscale Adv.* **2021**, *3*, 3799.
- [13] S. S. Staniland, B. Ward, A. Harrison, G. van der Laan, N. Telling, *Proc. Natl. Acad. Sci. USA* **2007**, *104*, 19524.
- [14] E. Alphanđery, *Front. Bioeng. Biotechnol.* **2014**, *2*, 5.
- [15] M. Amor, V. Busigny, M. Durand-Dubief, M. Tharaud, G. Ona-Nguema, A. Gélabert, *Proc. Natl. Acad. Sci. USA* **2015**, *112*, 1699.
- [16] S. S. Staniland, A. E. Rawlings, *Biochem. Soc. Trans.* **2016**, *44*, 883.
- [17] N. Nakamura, J. G. Burgess, K. Yagiuda, S. Kudo, T. Sakaguchi, T. Matsunaga, *Anal. Chem.* **1993**, *65*, 2036.
- [18] F. Mickoleit, D. Schüler, *Adv. Biosyst.* **2018**, *2*, 1700109.
- [19] Y. Zhu, T. Mei, Y. Wang, Y. Qian, *J. Mater. Chem.* **2011**, *21*, 11457.
- [20] M. A. Vetten, C. S. Yah, T. Singh, M. Gulumian, *Nanomed.: Nanotechnol. Biol. Med.* **2014**, *10*, 1391.
- [21] E. Alphanđery, *Drug Discovery Today* **2020**, *25*, 1444.
- [22] L. Xiang, J. Wei, S. Jianbo, W. Guili, G. Feng, L. Ying, *Letts. Appl. Microbiol.* **2007**, *45*, 75.
- [23] X. Nan, W. Lai, D. Li, J. Tian, Z. Hu, Q. Fang, *Nanomaterials* **2021**, *11*, 1235.
- [24] J. Cypriano, J. Werckmann, G. Vargas, A. Lopes dos Santos, K. T. Silva, P. Leão, F. P. Almeida, D. A. Bazylnski, M. Farina, U. Lins, F. Abreu, *PLoS One* **2019**, *14*, e0215657.
- [25] G. Vargas, J. Cypriano, T. Correa, P. Leão, D. A. Bazylnski, F. Abreu, *Molecules* **2018**, *23*, 2438.
- [26] J. B. Sun, T. Tang, J. Duan, P. Xu, Z. Wang, Y. Zhang, L. Wu, Y. Li, *Nanotoxicology* **2010**, *4*, 271.
- [27] S. Rosenfeldt, F. Mickoleit, C. Jörke, J. H. Clement, S. Markert, V. Jérôme, S. Schwarzingler, R. Freitag, D. Schüler, R. Uebe, A. S. Schenk, *Acta Biomater.* **2021**, *120*, 293.
- [28] H. T. Phan, A. J. Haes, *J. Phys. Chem. C* **2019**, *123*, 16495.
- [29] O. Raschdorf, D. Schüler, R. Uebe, in *Microbial Proteomics*, (Ed: D. Becher), Humana Press, New York, NY **2018**, Ch. 5.
- [30] J. Xu, J. Hu, L. Liu, L. Li, X. Wang, H. Zhang, W. Jiang, J. Tian, Y. Li, J. Li, *Front. Microbiol.* **2014**, *5*, 136.
- [31] F. Mickoleit, C. B. Borkner, M. Toro-Nahuelpan, H. M. Herold, D. S. Maier, J. M. Pitzko, T. Scheibel, D. Schüler, *Biomacromolecules* **2018**, *19*, 962.
- [32] F. Mickoleit, S. Rosenfeldt, M. Toro-Nahuelpan, M. Schaffer, A. S. Schenk, J. M. Pitzko, D. Schüler, *Adv. Biol.* **2021**, *5*, 2101017.
- [33] F. Mickoleit, C. Lanzloth, D. Schüler, *Small* **2020**, *16*, 1906922.
- [34] A. Scheffel, A. Gärdes, K. Grünberg, G. Wanner, D. Schüler, *J. Bacteriol.* **2008**, *190*, 377.
- [35] H. Nudelman, R. Zarivach, *Front. Microbiol.* **2014**, *5*, 9.
- [36] R. Uebe, K. Junge, V. Henn, G. Poxleitner, E. Katzmann, J. M. Pitzko, R. Zarivach, T. Kasama, G. Wanner, M. Pósfai, L. Böttger, B. Matzanke, D. Schüler, *Mol. Microbiol.* **2011**, *82*, 818.
- [37] R. Puri, V. Arora, A. Kabra, H. Dureja, S. Hamaal, *J. Nanomater.* **2022**, *2022*, 6414585.
- [38] T. Friedrich, T. Lang, I. Rehberg, R. Richter, *Rev. Sci. Instrum.* **2012**, *83*, 045106.
- [39] a) I. Rehberg, R. Richter, S. Hartung, N. Lucht, B. Hankiewicz, T. Friedrich, *Phys. Rev. B* **2019**, *100*, 134425; b) I. Rehberg, R. Richter, S. Hartung, *J. Magn. Magn. Mater.* **2020**, *508*, 166868.

- [40] R. E. Rosensweig, *Ferrohydrodynamics*, Cambridge University Press, Cambridge **1985**.
- [41] B. Berkovski, V. Bastovoy (Eds), *Magnetic Fluids and Application Handbook*, edn. 1, Begell House, Inc., New York **1984**.
- [42] J. Curiale, M. Granada, H. E. Troiani, R. D. Sánchez, A. G. Leyva, P. Levy, K. Samwer, *Appl. Phys. Lett.* **2009**, 95, 043106.
- [43] M. Widdrat, M. Kumari, É. Tompa, M. Pósfai, A. M. Hirt, D. Faivre, *ChemPlusChem* **2014**, 79, 1225.
- [44] Z. Shaterabadi, G. Nabiyouni, G. F. Goya, M. Soleymani, *Appl. Phys. A* **2022**, 128, 631.
- [45] DIN Deutsches Institut für Normen e.V. Biologische Beurteilung von Medizinprodukten - Teil 5: Prüfungen auf in vitro-Zytotoxizität (ISO 10993-5:2009); Deutsche Fassung EN ISO 10993-5:2009, www.din.de (accessed: October 2022).
- [46] T. L. Moore, L. Rodriguez-Lorenzo, V. Hirsch, S. Balog, D. Urban, C. Jud, B. Rothen-Rutishauser, M. Lattuada, A. Petri-Fink, *Chem. Soc. Rev.* **2015**, 44, 6287.
- [47] F. Zhang, L. J. Zhao, S. M. Wang, J. Yang, G. H. Lu, N. N. Luo, X. Y. Gao, G. H. Ma, H. Y. Xie, W. Wei, *Adv. Funct. Mater.* **2018**, 28, 1703326.
- [48] A. J. Ruys, Y. W. Mai, *Mater. Sci. Eng. A* **1999**, 265, 202.
- [49] P. Tartaj, M. del Puerto Morales, S. Veintemillas-Verdaguer, T. González-Carreño, C. J. Serna, *J. Phys. D: Appl. Phys.* **2003**, 36, R182.
- [50] A. Z. Wilczewska, K. Niemirowicz, K. H. Markiewicz, H. Car, *Pharmacol. Rep.* **2012**, 64, 1020.
- [51] E. Alphanbéry, A. T. Ngo, C. Lefèvre, I. Lisiecki, L. F. Wu, M. P. Pileni, *J. Phys. Chem. C* **2008**, 112, 12304.
- [52] E. Ren, Z. Lei, J. Wang, Y. Zhang, G. Liu, *Adv. Ther.* **2018**, 1, 1800080.
- [53] T. Nanda, A. Rathore, D. Sharma, *Front. Mater. Sci.* **2020**, 14, 387.
- [54] Y. Hamdous, I. Chebbi, C. Mandawala, R. Le Fèvre, F. Guyot, O. Seksek, E. Alphanbéry, *J. Nanobiotechnol.* **2017**, 15, 74.
- [55] S. Mannucci, S. Tambalo, G. Conti, L. Ghin, A. Milanese, A. Carboncino, E. Nicolato, M. R. Marinozzi, D. Benati, R. Bassi, P. Marzola, A. Sbarbati, *Contrast Media Mol. Imaging* **2018**, 2018, 2198703.
- [56] J. B. Sun, J. H. Duan, S. L. Dai, J. Ren, Y. D. Zhang, J. S. Tian, Y. Li, *Cancer Lett.* **2007**, 258, 109.
- [57] L. Cheng, Y. Ke, S. Yu, J. Jing, *Int. J. Nanomed.* **2016**, 11, 5277.
- [58] A. Fischer, M. Schmitz, B. Aichmayer, P. Fratzl, D. Faivre, *J. R. Soc., Interface* **2011**, 8, 1011.
- [59] F. Mickoleit, K. Altintoprak, N. L. Wenz, R. Richter, C. Wege, D. Schüler, *ACS Appl. Mater. Interfaces* **2018**, 10, 37898.
- [60] E. Alphanbéry, S. Faure, O. Seksek, F. Guyot, I. Chebbi, *ACS Nano* **2011**, 5, 6279.
- [61] T. Revathy, M. A. Jayasri, K. Suthindhiran, *3 Biotech* **2017**, 7, 126.
- [62] S. Naqvi, M. Samim, M. Z. Abdin, F. J. Ahmed, A. N. Maitra, C. K. Prashant, A. K. Dinda, *Int. J. Nanomed.* **2010**, 5, 983.
- [63] D. Schüler, M. Köhler, *Zentralbl. Mikrobiol.* **1992**, 147, 150.
- [64] D. Schultheiss, D. Schüler, *Arch. Microbiol.* **2003**, 179, 89.
- [65] U. Heyen, D. Schüler, *Appl. Microbiol. Biotechnol.* **2003**, 61, 536.
- [66] T. Phenrat, N. Saleh, K. Sirk, R. D. Tilton, G. Lowry, *Environ. Sci. Technol.* **2007**, 41, 284.
- [67] A. Tiraferri, K. L. Chen, R. Sethi, M. Elimelech, *J. Colloid Interface Sci.* **2008**, 324, 71.
- [68] T. J. Collins, *BioTechniques* **2007**, 43, S25.
- [69] U. K. Laemmli, *Nature* **1970**, 227, 680.
- [70] S. P. Fling, D. S. Gregerson, *Anal. Biochem.* **1986**, 155, 83.
- [71] C. Lang, D. Schüler, *Appl. Environ. Microbiol.* **2008**, 74, 4944.
- [72] S. R. S. Rangan, *Cancer* **1972**, 29, 117.
- [73] A. K. Virmani, K. M. Fong, D. Kodagoda, D. McIntire, J. Hung, V. Tonk, J. D. Minna, A. F. Gazdar, *Genes, Chromosomes Cancer* **1998**, 21, 308.